

Non-van der Waals honeycomb antiferromagnet SrRu₂O₆ down to a few layers

Suvidyakumar Homkar,[†] Bharat Chand,[†] Shatruhan Singh Rajput,[†] Sandeep Gorantla,[‡] Tilak Das,[¶] Rohit Babar,[†] Shivprasad Patil,^{†,||} Rüdiger Klingeler,^{§,⊥} Sunil Nair,^{†,||} Mukul Kabir,^{†,||} and Ashna Bajpai^{*,†,||}

[†]*Department of Physics, Indian Institute of Science Education and Research, Dr. Homi Bhabha Road, Pune 411008, India.*

[‡]*LUKASIEWICZ Research Network PORT-Polish Center for Technology Development, ul. Stabłowicka 147, 54-066 Wrocław, Poland.*

[¶]*Dipartimento di Scienza dei Materiali, Università di Milano, Bicocca, via R. Cozzi 55, 20125 Milano, Italy.*

[§]*Kirchhoff Institute of Physics, Heidelberg University, INF 227, 69120 Heidelberg, Germany.*

^{||}*Centre for Energy Science, Indian Institute of Science Education and Research, Dr. Homi Bhabha Road, Pune 411008, India.*

[⊥]*Centre for Advanced Materials, Heidelberg University, INF 225, 69120 Heidelberg, Germany.*

E-mail: ashna@iiserpune.ac.in

Phone: +91 (20) 2590 8107. Fax: +91 (20) 2025 1566

Abstract

The current family of experimentally realized two-dimensional magnetic materials consist of 3d transition metals with very weak spin-orbit coupling. In contrast, we report a new platform in a chemically bonded and layered 4d oxide, with strong electron correlations and competing spin-orbit coupling. We synthesize ultra-thin sheets of SrRu₂O₆ using scalable liquid exfoliation. These exfoliated sheets are characterized by complementary experimental and theoretical techniques. The thickness of the nano-sheets varies between three to five monolayers, and within the first-principles calculations, we show that antiferromagnetism survives in these ultra-thin layers. Experimental data suggest that exfoliation occurs from the planes perpendicular to the *c*-axis as the intervening hexagonal Sr-lattice separates the two-dimensional magnetic honeycomb Ru-layers. The high-resolution

transmission electron microscope images indicate that the average inter-atomic spacing between the Ru-layers is slightly reduced, which agrees with the present calculations. The signatures of rotational stacking of the nanosheets are also observed. Such new two-dimensional platform offers enormous possibilities to explore emergent properties that appear due to the interplay between magnetism, strong correlations and spin-orbit coupling. Moreover, these effects can be further tuned as a function of layer thickness.

Introduction

The continuous rotational symmetry of spins prevents any long-range magnetic ordering in the isotropic Heisenberg model in two-dimension, as described by the celebrated Hohenberg-Mermin-Wagner theorem.^{1,2} The

long-wavelength excitations become gapless, and thus any tendency to magnetic order is destroyed at finite temperature. However, spins in real materials are far from being isotropic, and the dipolar interaction or relativistic spin-orbit coupling produces magnetic anisotropy, which breaks the continuous rotational invariance of the spins. Therefore, the excitation becomes gapped, and a magnetic phase transition emerges in two-dimension. Unfortunately, despite its immense importance, it is rare to find two-dimensional magnetic materials with strong spin-orbit coupling.^{3,4}

The recent discovery of antiferromagnetic ordering in FePS₃ together with the ferromagnetic ordering in CrGeTe₃ and CrI₃ are the first-ever demonstration of magnetic order in truly two-dimensional materials.⁵⁻⁷ This breakthrough marks a new era in fundamental research along with enormous application possibilities in two dimensions, and extend functionalities beyond the already existing phases such as ferroelectricity, superconductivity, charge density waves, and various topological states. Apart from these materials, a few other ferromagnetic materials CrCl₃, CrBr₃, VI₃, VSe₂, Fe₃GeTe₂ and MnBi₂Te₂; and antiferromagnet like NiPS₃ have been discovered.⁸⁻¹⁴ Further, electric manipulation of magnetism has been achieved in these two-dimensional materials, that opens up opportunities in spintronic applications.^{13,15,16} It is important to note here that all the materials that are discovered till date are derived from the van der Waals bulk materials and consists of 3*d* transition-metals that have weak spin-orbit coupling strength.^{3,4} Since the anisotropic interactions originating from the spin-orbit coupling opens a gap in the spin-wave spectrum, the corresponding magnetic transition temperature is undesirably low in these materials.¹⁷ Therefore, it would be exciting to discover a new class of two-dimensional magnets with much stronger spin-orbit couplings that couple with strong electron correlation. The interplay between these competing interactions at the comparable energy scales along with the band topology is expected to trigger emergent physics and exciting functionalities in two-dimensional materials.

Transition metal oxides with the 4*d* and 5*d* elements are the prime examples of such competing interactions with comparable electron correlation and spin-orbit coupling.^{18,19} Consequently, many exotic physics have been discovered in these oxides in their bulk phases. For example, spin-triplet superconductivity²⁰ and emergent Higgs mode oscillations have been discovered in the ruthenium-based materials.^{21,22} In the context of two-dimensional magnetism, the difficulty in exfoliation of these non-vdW materials is the main obstacle. While the magnetism in many of these oxides appears in layers, these magnetic layers are chemically bonded with one another, which makes exfoliation a challenging task.

Another bottleneck that prevents the use of these 4*d* and 5*d* transition metal oxides in multifunctional devices is that the magnetic transition temperatures of most of these oxides are far below room temperature. Only a very few 4*d* and 5*d* oxides, such as CaTcO₃,²³ SrTcO₃,²⁴ NaOsO₃^{25,26} and Sr₃OsO₆,²⁷ have been discovered to have very high magnetic ordering temperatures but none of these materials displays layered magnetic structure. Hence, the realization of strongly correlated oxides with high transition temperatures is an area of intense theoretical and experimental investigations. In this context, the recent discovery of SrRu₂O₆ with high Neel temperature T_N of 560 K is of great importance,^{28,29} which also holds some exotic electronic properties owing to both localized and itinerant character of electrons.^{30,31} Bulk SrRu₂O₆ is a layered antiferromagnetic insulator with honeycomb magnetic lattice of Ru⁵⁺ ions and the properties could be further tailored by inducing strain in the lattice to host topological states.^{28,29,32,33} Therefore, the layered SrRu₂O₆ is a potential candidate for exfoliation, and consequently for experimental realization of two-dimensional magnetism in strongly correlated oxides.

Here, we report the synthesis of ultra-thin sheets of SrRu₂O₆ using the scalable technique of liquid exfoliation. These nano-sheets are formed and preserved in the liquid medium of ethanol, which enables easy drop-casting on a suitable substrate for further characteriza-

tion and device patterning. The ultra-thin sheets are characterized by a wide range of complementary experimental and theoretical techniques. Experimental results indicate stable nano-sheets with the thickness between three to five monolayers. The theoretical calculations suggest the survival of antiferromagnetism in these nano-sheets. Therefore, these few-layer oxide sheets serve as the new platform beyond the current family of two-dimensional magnetic materials, which additionally host electron correlation and spin-orbit coupling at competing scales. Moreover, the strongly correlated electrons on the hexagonal lattice with antiferromagnetic interactions provide a fertile playground for emergent phenomena.^{34–36} In this context, SrRu₂O₆ is also quite similar to the celebrated RuCl₃^{37,38} and Na₂IrO₃ systems,³⁹ in which Ru or Ir ions form a magnetic hexagon with antiferromagnetic correlations. Both these systems are extensively explored for the possibility of hosting fractionalized Kitaev physics with unconventional excitations.^{39–44}

Experimental Techniques

SrRu₂O₆ crystallites are synthesized via the hydrothermal route, using an autoclave from Parr instruments. The morphology and size of as-synthesized bulk crystallites as well as the nano-sheets of the same, are recorded using a Zeiss Ultra plus FESEM. Powder X-ray diffraction (XRD) on the crystallites have been conducted using Bruker D8 Advance with Cu K_{α} radiation ($\lambda = 1.54056 \text{ \AA}$). Raman spectroscopy has been done using Horiba instruments equipped with a blue laser ($\lambda = 488 \text{ nm}$) and a confocal microscope. The nano-sheets are characterized by Transmission Electron Microscopy (FEI/TFS Tecnai 20, equipped with LaB6 electron gun, operated at 200 kV). TEM specimens are prepared by drop casting a few μL of solution of SrRu₂O₆ nano-sheets, dispersed and preserved in ethanol, onto Cu TEM grids coated with amorphous carbon support film. The Selected Area Electron Diffraction patterns (SAED) and Fast Fourier Transform (FFT) diffractograms are analyzed by ELDISCA soft-

ware.⁴⁵ The nano-sheets are further characterized using Atomic Force Microscopy (AFM) using JPK Nanowizard II. For the synthesis of SrRu₂O₆ nano-sheets, sonicator (Model Bandelin Sonorex RK 100 H) and Hettich centrifuge (Model MIKRO 200-R) has been used.

The process of liquid exfoliation is routinely employed to form ultra-thin sheets of graphene-like van der Waals materials, including a wide variety of chalcogenides such as MoS₂.^{46–49} This process involves finding a suitable liquid medium in which the bulk sample is sonicated and centrifuged. Here important synthesis parameters include (i) sonication which enables separation of layers which are weakly bonded (ii) centrifugation which enables isolation of thin sheets. The suitable choice of liquid medium is important, as it prevents the isolated nano-sheets from coagulating again. Time of sonication and centrifugation are also crucial parameters that can be tuned to further refine the thickness distribution as well as size of the nano sheets.^{46–49} While a large number of layered van der Waals materials have been successfully exfoliated using this technique, there are relatively few reports^{50–53} of exfoliation of magnetic oxides, especially layered ones, with high spin-orbit coupling. Oxides such as SrRu₂O₆ are quasi two dimensional in the sense of weak inter-layer bonding as compared to in-plane bonding, though both inter-plane and intra-layer bonding are covalent in nature. This anisotropy in bonding strength can thus be exploited to exfoliate ultra-thin sheets of non van der Waals but layered systems, using the technique of liquid exfoliation.

Results and Discussions

The compound SrRu₂O₆, crystallizes in a quasi-2D structure with space group $P\bar{3}1m$ and lattice parameters $a = 0.520573 \text{ nm}$, $c = 0.523454 \text{ nm}$.³³ As shown in Figure 1(a), the structure of SrRu₂O₆ comprises of edge-sharing RuO₆ layers separated by Sr²⁺ ions. Within the ab plane, the Ru ions are arranged in a honeycomb structure and Ru moments couple antiferromagnetically both in-plane and out-of-plane. The mag-

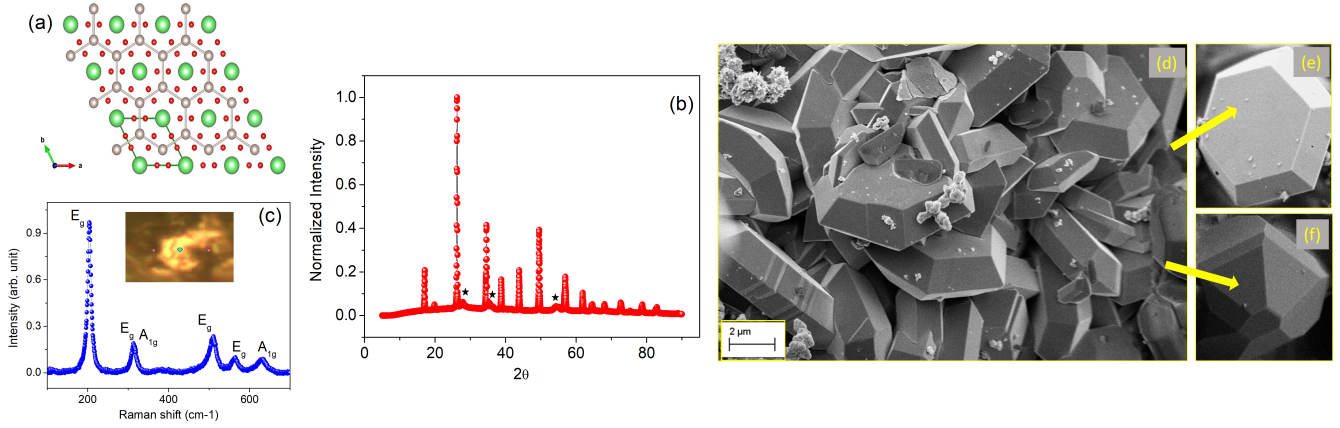


Figure 1: (a) Schematic of a honeycomb lattice of Ru ions (gray balls) in the ab plane. The Ru layers are separated by Sr layers (green balls) along the c axis. (b) depicts room temperature powder XRD data for SrRu_2O_6 synthesized using the hydrothermal method. Here the intensity has been normalized with the most intense peak of SrRu_2O_6 . A tiny impurity of RuO_2 is marked by stars. (c) shows the Raman data, obtained on a crystallite of SrRu_2O_6 , with the optical image for the crystallite being shown in the inset. The morphology of the sample is depicted in the SEM image of bulk SrRu_2O_6 as shown in (d), which depicts an overall view of micron-size crystallites forming in regular morphology. (e) and (f) are images of isolated hexagonal crystallites and regular polyhedra. The liquid exfoliation technique has been employed to obtain ultra-thin sheets of SrRu_2O_6 , using these regular shaped crystallites shown in (d) to (f).

netic moment is $1.30 \mu_B/\text{Ru}$ at room temperature and the system possesses the G-type magnetic structure.^{29,33}

For obtaining the nano-sheets, we first synthesize bulk SrRu_2O_6 employing the hydrothermal technique described earlier.³³ For this purpose, KRuO_4 and SrO_2 (in stoichiometric ratios) are added in distilled water and stirred, prior to heating the mixture at 200 C for 24 hours in an autoclave. The precipitate was recovered using a vacuum filtration assembly and washed with diluted HCl, distilled water and acetone. The sample thus obtained was characterized by XRD and Raman, as is shown in Figure 1(b) and Figure 1(c), respectively. The XRD pattern matches well with, JCPDS (04-021-3995) entry assigned for SrRu_2O_6 .³³ The lattice parameters derived from XRD data are $a = 0.5205(7)$ nm, $c = 0.5219(5)$ nm. A tiny amount of RuO_2 phase, JCPDS (65-2824), is also observed as marked by stars in Figure 1(b). This impurity could be systematically reduced by repeated washing the *as-prepared* compound and does not interfere in the exfoliation of SrRu_2O_6 . A characteristic Raman spectra ac-

quired using blue laser is shown in the main panel of Figure 1(c). The inset shows the optical image of the crystallite, on which the Raman data has been recorded. The Raman data shown in Figure 1(c) are consistent with the previous reports.⁵⁴ . Magnetic Characterization on SrRu_2O_6 crystallites is conducted using SQUID magnetometry (Quantum Design MPMS) and magnetization as function of temperature from 5K to 600 K is presented in Supp.Info Figure S1. The magnetization data are in agreement with previous reports^{29,33} and further confirm the phase purity of the parent compound used for the process of liquid exfoliation. The morphology of the SrRu_2O_6 depicting micron-size crystallites observed with regular facets, vertices and edges is shown in Figure 1(d)-(f). It is to be noted that a large number of crystallites are formed in regular hexagonal shape as is highlighted in Figure 1(e).

To obtain nano-sheets of SrRu_2O_6 , the first task is to determine a suitable liquid medium, in which the bulk crystallites can be dispersed. This solution, containing the bulk crystallites (in an optimized liquid-medium and crystallite

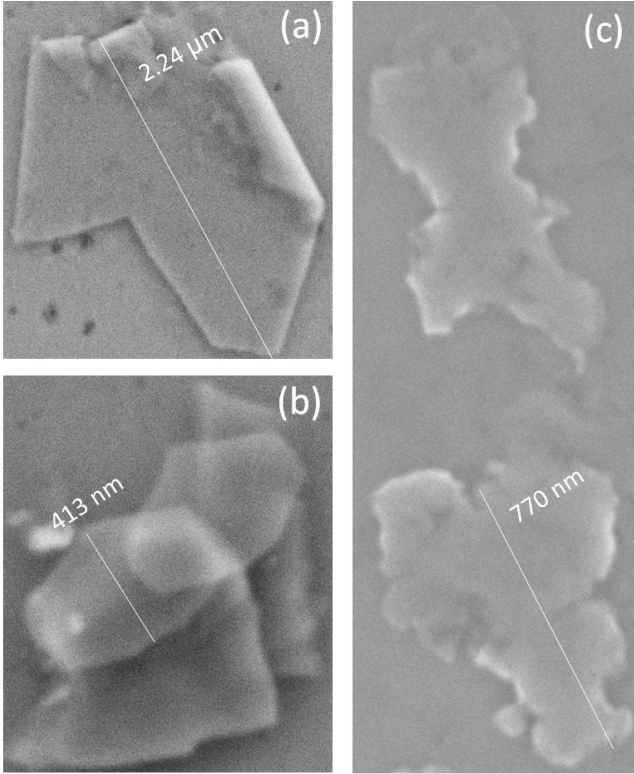


Figure 2: (a)–(c) are SEM images of thin flakes of SrRu_2O_6 , post the process of liquid exfoliation, indicating that sheets of various thickness and shapes have been formed. These images are recorded after drop casting the exfoliated sample on Si substrates.

ratio) is then subjected to sonication for mechanically isolating the weakly bonded layers. After trying a number of solvents, we found that ethanol is most suitable for obtaining ultra-thin sheets of SrRu_2O_6 . For this purpose, as-prepared SrRu_2O_6 crystallites were dispersed in ethanol. Usage of ethanol as a solvent for the process of liquid exfoliation has certain advantages. For instance, nano-sheets preserved in ethanol are easy to drop-cast on a suitable substrate. As ethanol evaporates, this provides an opportunity for easy device patterning. In order to synthesize ultra-thin sheets, we first make a solution of SrRu_2O_6 crystallites in ethanol, typically in a 1:10 ratio. This solution is subjected to 4 hours of bath and probe sonication, following which the solution is kept undisturbed for 24 hours. The top portion of the solution is collected and centrifuged at 2000 rpm for 30 minutes. These experimental parameters (such as time of sonication or

centrifugation etc.) can be further refined to obtain thinner nano-sheets. For instance, multiple rounds of sonication and centrifuge usually leads to the collection of relatively thinner sheets in the top portion of the centrifuge vial. The centrifuge vial is also kept undisturbed for a few hours prior to retrieving a few μL from the top layer using a micro pipette. This refined solution is then drop-cast onto the various suitable substrates for further characterization.

The Figures 2(a)–(c) displays SEM images of the nano-sheets thus formed. The images are recorded by drop-casting a few μL of the solution, that contains dispersed nano sheets, on a Si substrate. As evident from Figure 2, the sheets are formed in various shapes and size, for which a few representatives are shown here. Most importantly, we observe a significant fraction of sheets retain the shape of regular polyhedra of *as-formed* micro-crystals shown in Figure 1(d). Both isolated as well as a bunch of nano-sheets (which lie on top of each other) can be found. The lateral length of such nano-sheets varied from few tens of nano meters to a few 100 nm and again appears to correlate with dimensions of the bulk SrRu_2O_6 crystallites, from which these sheets have been exfoliated.

While the presence of sheets with different thicknesses can be gauged from the contrast in the SEM images, we performed AFM measurements for determining the average thickness of the nano sheets. For this purpose, solution containing dispersed nano -sheets is drop-casted on a freshly cleaved mica substrate. The Figures 3(a)–(d) show some representative AFM images on the nano-sheets of SrRu_2O_6 . The Figure 3(a) shows a broad area AFM image, displaying a large number of sheets of various shape and size on the substrate - also demonstrating the scalability which the technique of liquid exfoliation provides. This also grants us means to pick the sheets with desired thickness for future magnetotransport measurements. Many of the individual nano-sheets, such as shown in Figure 3(a), retain the shape of the bulk crystallites, used in the exfoliation. This is evident from AFM images shown in Figure 3(b)–(c), which show some neatly

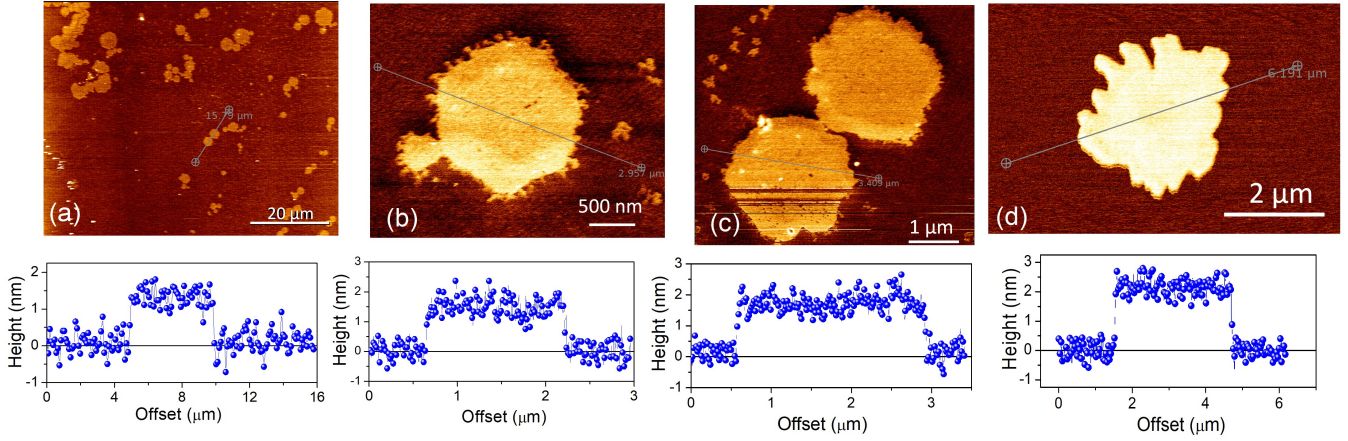


Figure 3: (a) - (d) are AFM images of the SrRu_2O_6 nano sheets of different shape and thickness drop-cast on a mica substrate. (a) cover a broad area, depicting a large number of nano flakes. Both isolated and agglomerated nano-sheets can be clearly seen here. (b) shows a hexagonal shaped nano flake, depicting the morphology of the as-prepared bulk SrRu_2O_6 shown in Figure 1. The average thickness of the individual nano-sheet is in the range of 1.5 to 2.2 nm, as is evident from the corresponding line profile shown at the bottom of (a) to (d).

formed hexagonal sheets, and a rather distorted hexagon. A fairly arbitrary shape sheet is shown in Figure 3(d) which bears striking similarities in SEM images shown for arbitrary shaped sheets in Figure 3(c).

From the AFM images presented in Figure 3(a), we estimated average thickness of sheets ~ 1.31 nm (± 0.12 nm), taking into account about 30 different sheets. The thickness of the hexagonal shaped sheets shown in Figure 3(b)-(c) is ~ 1.5 nm, whereas it is ~ 2.2 nm for the sheet shown in Figure 3d. Considering that the process of liquid exfoliation enables termination of sheets from Sr layer, the number of layers in perfectly stacked sheets can be gauged by looking into the lattice parameter $c = 0.523$ nm, corresponding to bulk SrRu_2O_6 . This approach suggests three to five monolayers, considering a significant reduction in lattice parameter c from its bulk value. This is especially interesting, as prior density functional theory (DFT) calculations have suggested that strain mediated topological properties could be observed in samples with certain thickness.³²

We also observed that repeating the entire process of sonication and centrifugation (after leaving the dispersed nano-sheets for months in the vial) resulted in narrower distribution

of thickness. The dispersed nano sheets in the solution, even after prolonged time-periods, retained the morphology, such as shown in Figure 2. Furthermore, repeated process of sonication and centrifugation performed using the solution preserved in the same vial led to the observation of relatively thinner sheets. In all these samples, many regions with partially stacked sheets, such as shown in Figure 2(b), could also be found. Thus it is evident that the each step involved in the process of liquid exfoliation, including the time of sonication and centrifugation can be further refined to obtain either monolayers or fully/partially stacked nano-sheets.

Exploring novel electronic states in van der Waals driven 2D materials, especially graphene is an area of extensive research⁵⁵⁻⁵⁷. However, antiferromagnetic interactions in a system with magnetic honeycomb and large spin orbit coupling is a testbed for exploring topological states. This is especially so in the case of SrRu_2O_6 , where DFT predicts strain mediated topological state and band inversion when the crystallographic c axis could be significantly tailored, leaving the a and b lattice parameters relatively unchanged.³² It is evident here that the nano-sheets of SrRu_2O_6 produced using the

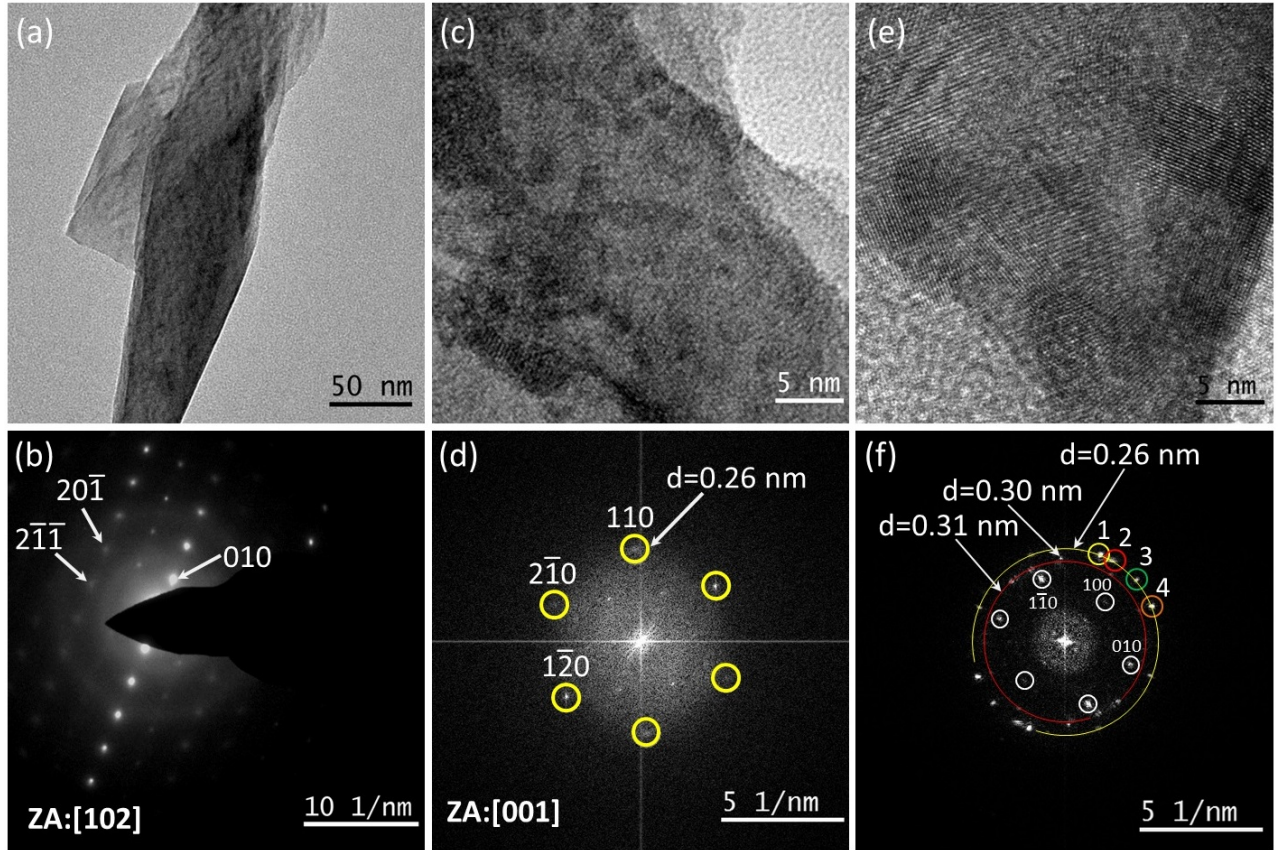


Figure 4: TEM, SAED and HRTEM characterization of the exfoliated SrRu_2O_6 flakes. (a) and (b) show an overview TEM image and corresponding SAED pattern of an exfoliated flake respectively. The diffraction pattern is indexed in agreement with $[102]$ zone axis of SrRu_2O_6 . (c) and (d) show a HRTEM image and corresponding FFT of an area at the edge of a few-layer flake respectively. The hexagonal symmetry of the spots in the FFT, marked by circles, is indexed in agreement with $[001]$ zone axis of SrRu_2O_6 . (e) and (f) show HRTEM image and corresponding FFT respectively of an area at the edge of another few-layer flake. In this FFT, multiple spots with 0.26 nm and 0.31 nm d-spacing are marked with outer and inner partial circle respectively. The spot corresponding to 0.30 nm d-spacing (bulk Ru-Ru spacing in $[001]$ projection) is marked by an arrow. The spots in FFT marked by numbered circles originate from four different regions at the edges of the flake in the corresponding HRTEM image, where (110) planes are rotated with respect to each other. The inner skewed hexagonal spots close to center of FFT, marked by white circle markers are indexed with $[001]$ zone axis SAED of SrRu_2O_6 crystal structure. The $(1-10)$ and (010) spots in the FFT are observed to deviate away from bulk crystal SAED pattern positions. This may be due to shrinking of the d-spacing of these planes in the real space after exfoliation.

technique of liquid exfoliation possibly provides a means to obtain ultra-thin 2D sheets, of various thickness and lateral lengths. From SEM and AFM images shown in Figure 2 and Figure 3, it is evident that these 2D sheets can range from a few 100 nm to a few microns. Thus, depending on the size and the thickness of the nano-sheet, both a as well as c lattice parameters can be strained anisotropically. For

instance, a monolayer which extends to a few microns in length, the c parameter is likely to be more strained than a lattice parameter. Experimental realization of such nano-sheets with varying thickness and lateral length also enables a possibility in which a particular lattice parameter (perpendicular to the weakly bonded layers) can be tuned, without significantly disturbing the (in-plane) lattice parameters. Such

2D sheets of SrRu_2O_6 can provide an opportunity to test the theoretical predictions, such as discussed in reference 32.

A representative overview TEM image of an individual flake is shown in Figure 4(a). It shows portion of a typical folded sheet of SrRu_2O_6 , which is about 100 nm wide and a few 100 nm long. The corresponding SAED pattern obtained from this sheet, as shown in Figure 4(b), could be indexed in agreement with the [102] zone axis diffraction pattern of SrRu_2O_6 . Figure 4(c) shows HRTEM image from an edge of the exfoliated nano-flake. In this image, atleast three different nano sheets edges can be seen. The FFT of this image in Figure 4(d) shows the spots in agreement with the hexagonal spot pattern of [001] zone axis Selected Area Electron diffraction (SAED) pattern of SrRu_2O_6 . The measured d-spacing from these spots, 0.26 nm, is in good agreement with the (110), (2-10) and (1-20) planes spacing of $d = 0.2603$ nm (from JCPDS card entry 04-021-3995 for SrRu_2O_6). This observation not only confirms that these crystalline nano -sheets have retained the bulk phase but also suggests that the nano-sheets may have been exfoliated from planes perpendicular to the c -axis of this system.

Figure 4(e) shows HRTEM image from a region of another flake, where some regions with moire pattern like contrast are observed. The corresponding FFT, Figure 4(f), shows FFT multiple spots with 0.26 nm d-spacing (supplementary figure TEM-S2), i.e. (110) planes as marked with outer partial circle. The spots that lie on this ring, as marked by numbered circles, originate from four different regions at the edges of the flake in the corresponding HRTEM image where (110) planes are rotated with respect to each other. Presence of multiple spots along a ring with constant d-spacings is typical of SAED/FFT pattern from a polycrystalline sample with randomly oriented grains. However, this does not appear to be the case here and is reminiscent of prior observations in few layer 2D materials like graphene, where similar FFT patterns were observed due to rotational stacking faults.⁵⁸ To satisfy this condition each spot in the marked numbered cir-

cle should clearly show a set of corresponding hexagonal spots which are not clearly observed in Figure 4(f). Thus, we can speculate that the pattern observed here may point towards the presence of stacked exfoliated sheets with different azimuthal rotation between them. However, it is worth noting that such a possibility of rotationally stacked nano-sheets is highly likely in this sample, as this tendency is also observed seen in SEM images, Figure 2(b).

In Figure 4(f), the spot corresponding to 0.30 nm d-spacing (bulk Ru-Ru spacing in [001] projection of SrRu_2O_6) is marked by an arrow, below which the multiple spots with constant d-spacing are marked with inner partial circles. The average spacing of the spots on this ring is measured to be 0.31 nm (supplementary figure TEM-S3). This observation indicate slight in plane shrinking of Ru-Ru interatomic spacing in the exfoliated nanosheets. Finally, in Figure 4(f), the six spots close to the center of FFT (as marked by white circle markers) show a distorted hexagonal arrangement. They are indexed with [001] zone axis SAED of SrRu_2O_6 crystal structure. The (1-10) and (010) spots in the FFT are observed to deviate away from their expected positions in simulated [001] zone axis SAED pattern positions. The measured d-spacing of these planes show an average spacing of 0.365 nm as compared to the bulk value of 0.45 nm. This indicates shrinking of the d-spacing of these planes after exfoliation. Also the measured d-spacing of 100 planes in the FFT (0.43 nm) indicate slight decrease of the inter planar spacing between them (supplementary Figure S4). We believe that strain effects in lattice parameters upon exfoliating a non van der Waals but layered system such as SrRu_2O_6 , are likely to be larger. TEM data presented here is indicative of large strain effects as observed in these nano sheets. We also recorded EDX in TEM on a number of 2D nano-sheets, a representative of which is shown as Figure S5 in the supplementary information.

To gain further insights, about the electronic structure, we characterize the SrRu_2O_6 nano-sheets within the first-principles density functional theory (DFT) calculations as implemented in the Vienna Ab Initio Simula-

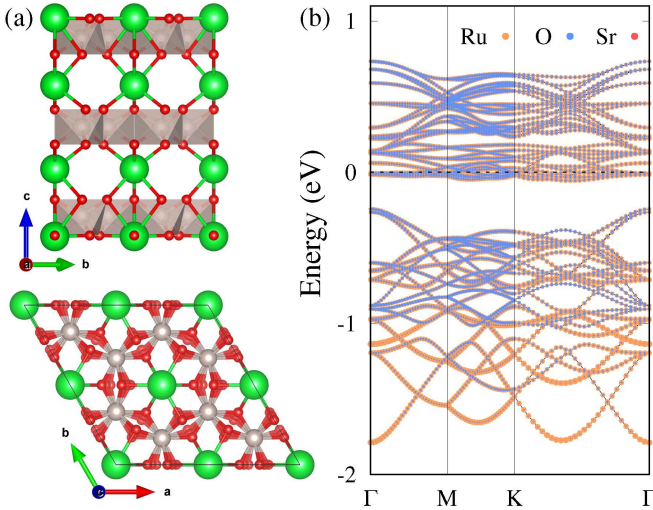


Figure 5: (a) Top and side views of the optimized lattice of 3L SrRu_2O_6 ultrathin film. The surface Sr-layer relaxes toward the RuO_6 octahedra, and the O-positions indicate distortion in the RuO_6 octahedra at the surface. (b) Band dispersion of the 3L SrRu_2O_6 in the G-type antiferromagnetic magnetic structure exhibit metallic character. The Fermi energy is set to $E = 0$. The metallic solution remains invariant in the non-magnetic state, and also when the spin-orbit coupling is incorporated in the calculation.

tion Package.^{59,60} The wave function is described within the projector augmented wave formalism with 500 eV kinetic energy cut-off.⁶¹ The exchange-correlation is treated with the Perdew-Burke-Ernzerhof functional,⁶² and the spin-orbit coupling is treated self-consistently. A large vacuum of 17 Å is maintained perpendicular to the surface of the few-layer SrRu_2O_6 nano-sheet to minimize the spurious interaction between the periodic images. The structure is completely relaxed until the forces reduce below ± 0.01 eV/Å threshold. The Brillouin zone is sampled using a $9 \times 9 \times 9$ and $9 \times 9 \times 1$ k -mesh for the bulk and few-layered samples, respectively.

Before we discuss the structural, electronic and magnetic properties of the ultrathin SrRu_2O_6 nano-sheet, we revisit the intriguing bulk phase within the same theoretical hierarchy. The calculated lattice parameters ($a = 5.29$ and $c = 5.26$ Å) are in good agreement

with the experimental values calculated from the neutron diffraction data.³³ The Ru^{5+} -ions in the hexagonal $P\bar{3}1m$ lattice of SrRu_2O_6 are octahedrally coordinated with the oxygen ions, which supports the half-filled t_{2g} -manifold with $3 \mu_B$ expected moment. However, due to the strong hybridization between Ru- t_{2g} and O- $2p$ orbitals, the Ru-moment is substantially reduced to $1.38 \mu_B$, in agreement with prior experimental and theoretical results.^{29,30,44,63–66} The two-dimensional Ru-spins exhibit G-type antiferromagnetic with semiconducting electronic structure. The corresponding non-magnetic solution indicates a small bandgap of 68 meV in the present calculation, while the gap increases with the Ru-moment.⁴⁴ We find the G-type antiferromagnetic SrRu_2O_6 to have a higher 0.44 eV gap, and the inclusion of spin-orbit coupling does not further influence the gap (0.41 eV).

The structure of the Sr-terminated 3L SrRu_2O_6 sheet is fully relaxed [Figure 5(a)], and the in-plane lattice parameter a is slightly stretched (5.38 Å), in comparison to the corresponding bulk value. In contrast, the perpendicular lattice parameter c is critically contracted in 3L SrRu_2O_6 (4.27 Å compared to 5.26 Å in bulk) due to the relaxation of surface Sr-layer toward the RuO-octahedra, which is in remarkable agreement with the experimental observations, particularly the AFM and TEM measurements presented in Figure 3, Figure 4 and supplementary Figure S3. These data bring out significant strain effects in the interlayer spacing, which leads to associated compression or expansion in the lattice parameters of SrRu_2O_6 nano-sheets.

Similar to the bulk, the ultra-thin SrRu_2O_6 sheet exhibits G-type antiferromagnetic ordering, which is 30 meV/Ru lower in energy compared to the corresponding ferromagnetic state. The individual Ru-moments decreases to $1.32 \mu_B$ at the middle RuO-layer, which further reduces at the surface due to RuO_6 distortion. Surprisingly, an insulator to metal transition is observed while the thickness is reduced to few-layer [Figure 5(b)]. The 3L SrRu_2O_6 sheet is found to be metallic, which is mostly contributed by the $p-d$ hybridization at the dis-

torted surface RuO_6 octahedra. The predicted (antiferro) magnetism in the ultrathin SrRu_2O_6 nano-sheets will have implications in the search for magnetism in the two-dimension, that is typically observed in the van der Waals systems.³⁻⁷

Conclusions

In conclusion, we demonstrate a new platform to realize two-dimensional magnetism in non-van der Waals and magnetically layered $4d$ oxide with strong electron correlation and competing spin-orbit coupling. We exfoliate the ultra-thin nano-sheets of SrRu_2O_6 using the scalable technique of liquid exfoliation. While the method of liquid exfoliation was primarily meant for van der Waals materials like graphene, we show that the same technique can be successfully employed to obtain nano-sheets of inherently layered magnetic oxides such as SrRu_2O_6 , with anisotropic in-plane and out-of-plane bond strengths. These nano-sheets could be obtained and preserved using ethanol as a medium. This enables one to easily drop-cast them on a suitable substrate for characterization as well as on patterned substrates for magneto-transport measurements. Scanning and Transmission electron microscopy, as well as Atomic force microscopy, have been used to characterize these nano-sheets. Within the complementary first-principles calculations, we show that antiferromagnetism survives in these ultra-thin nano-sheets. Experimental realization of two-dimensional sheets of SrRu_2O_6 which has a graphene-like magnetic honeycomb, along with competing electronic correlations and spin-orbit coupling offers tremendous potential to investigate emergent phenomena in this particular type of two-dimensional magnets. The present study will incite further attention in this regard.

Acknowledgments

Authors acknowledge Prof. A.K.Nigam for useful discussions, Mr. Rudheer Bapat and Mr. J. Parmar for TEM measurements and Mr. A.

Shetty for SEM measurements. A.B. acknowledges Department of Science and Technology (DST), India for funding support through a Ramanujan Grant. A.B., S.N., M.K., and S.P. acknowledge DST Nanomission Thematic Unit Program for financial support. R.K., S.N. and A.B. acknowledge funding support through Joint DST-DFG projects INT/FRG/DFG/P-06/2017 and KL1824/11-1. M.K. acknowledges funding from the Science and Engineering Research Board through EMR/2016/006458 grant.

References

- (1) Hohenberg, P. C. Existence of Long-Range Order in One and Two Dimensions. *Phys. Rev.* **1967**, *158*, 383–386.
- (2) Mermin, N. D.; Wagner, H. Absence of Ferromagnetism or Antiferromagnetism in One- or Two-Dimensional Isotropic Heisenberg Models. *Phys. Rev. Lett.* **1966**, *17*, 1133–1136.
- (3) Gibertini, M.; Koperski, M.; Morpurgo, A. F.; Novoselov, K. S. Magnetic 2D materials and heterostructures. *Nat. Nanotechnol.* **2019**, *14*, 408–419.
- (4) Gong, C.; Zhang, X. Two-dimensional magnetic crystals and emergent heterostructure devices. *Science* **2019**, *363*.
- (5) Lee, J.-U.; Lee, S.; Ryoo, J. H.; Kang, S.; Kim, T. Y.; Kim, P.; Park, C.-H.; Park, J.-G.; Cheong, H. Ising-Type Magnetic Ordering in Atomically Thin FePS₃. *Nano Lett.* **2016**, *16*, 7433–7438.
- (6) Gong, C.; Li, L.; Li, Z.; Ji, H.; Stern, A.; Xia, Y.; Cao, T.; Bao, W.; Wang, C. e.; Wang, Y.; Qiu, Z. Q.; Cava, R. J.; Louie, S. G.; Xia, J.; Zhang, X. Discovery of intrinsic ferromagnetism in two-dimensional van der Waals crystals. *Nature* **2017**, *546*, 265.
- (7) Huang, B.; Clark, G.; Navarro-Moratalla, E.; Klein, D. R.; Cheng, R.;

- Seyler, K. L.; Zhong, D.; Schmidgall, E.; McGuire, M. A.; Cobden, D. H.; Yao, W.; Xiao, D.; Jarillo-Herrero, P.; Xu, X. Layer-dependent ferromagnetism in a van der Waals crystal down to the monolayer limit. *Nature* **2017**, *546*, 270.
- (8) Kim, H. H. et al. Evolution of interlayer and intralayer magnetism in three atomically thin chromium trihalides. *Proc. Natl. Acad. Sci. USA* **2019**, *116*, 11131–11136.
- (9) Wang, Z.; Gibertini, M.; Dumcenco, D.; Taniguchi, T.; Watanabe, K.; Gianini, E.; Morpurgo, A. F. Determining the phase diagram of atomically thin layered antiferromagnet CrCl₃. *Nat. Nanotechnol.* **2019**, *14*, 1116–1122.
- (10) Klein, D. R.; MacNeill, D.; Song, Q.; Larson, D. T.; Fang, S.; Xu, M.; Ribeiro, R. A.; Canfield, P. C.; Kaxiras, E.; Comin, R.; Jarillo-Herrero, P. Enhancement of interlayer exchange in an ultrathin two-dimensional magnet. *Nat. Phys.* **2019**, *15*, 1255–1260.
- (11) Kong, T.; Stolze, K.; Timmons, E. I.; Tao, J.; Ni, D.; Guo, S.; Yang, Z.; Prozorov, R.; Cava, R. J. VI₃?a New Layered Ferromagnetic Semiconductor. *Adv. Mater.* **2019**, *31*, 1808074.
- (12) Bonilla, M.; Kolekar, S.; Ma, Y.; Diaz, H. C.; Kalappattil, V.; Das, R.; Eggers, T.; Gutierrez, H. R.; Phan, M.-H.; Batzill, M. Strong room-temperature ferromagnetism in VSe₂ monolayers on van der Waals substrates. *Nat. Nanotechnol.* **2018**, *13*, 289–293.
- (13) Deng, Y.; Yu, Y.; Song, Y.; Zhang, J.; Wang, N. Z.; Sun, Z.; Yi, Y.; Wu, Y. Z.; Wu, S.; Zhu, J.; Wang, J.; Chen, X. H.; Zhang, Y. Gate-tunable room-temperature ferromagnetism in two-dimensional Fe₃GeTe₂. *Nature* **2018**, *563*, 94–99.
- (14) Kim, K.; Lim, S. Y.; Lee, J.-U.; Lee, S.; Kim, T. Y.; Park, K.; Jeon, G. S.; Park, C.-H.; Park, J.-G.; Cheong, H. Suppression of magnetic ordering in XXZ-type antiferromagnetic monolayer NiPS₃. *Nat. Commun.* **2019**, *10*, 345.
- (15) Huang, B.; Clark, G.; Klein, D. R.; MacNeill, D.; Navarro-Moratalla, E.; Seyler, K. L.; Wilson, N.; McGuire, M. A.; Cobden, D. H.; Xiao, D.; Yao, W.; Jarillo-Herrero, P.; Xu, X. Electrical control of 2D magnetism in bilayer CrI₃. *Nat. Nano.* **2018**, *13*, 544–548.
- (16) Jiang, S.; Li, L.; Wang, Z.; Mak, K. F.; Shan, J. Controlling magnetism in 2D CrI₃ by electrostatic doping. *Nat. Nano.* **2018**, *13*, 549–553.
- (17) Lado, J. L.; Fernández-Rossier, J. On the origin of magnetic anisotropy in two dimensional CrI₃. *2D Mater.* **2017**, *4*, 035002.
- (18) Khomskii, D. I. *Transition Metal Compounds*; Cambridge University Press, 2014.
- (19) Cox, P. *Transition Metal Oxides, An introduction to their electronic structure and properties*; Mayer J. et al. (Springer), 2010.
- (20) Maeno, Y.; Kittaka, S.; Nomura, T.; Yonezawa, S.; Ishida, K. Evaluation of Spin-Triplet Superconductivity in Sr₂RuO₄. *J. Phys. Soc. Jap.* **2012**, *81*, 011009.
- (21) Jain, A.; Krautloher, M.; Porras, J.; Ryu, G. H.; Chen, D. P.; Abernathy, D. L.; Park, J. T.; Ivanov, A.; Chaloupka, J.; Khaliullin, G.; Keimer, B.; Kim, B. J. Higgs mode and its decay in a two-dimensional antiferromagnet. *Nat. Phys.* **2017**, *13*, 633.
- (22) Souliou, S.-M.; Chaloupka, J. c. v.; Khaliullin, G.; Ryu, G.; Jain, A.; Kim, B. J.; Le Tacon, M.; Keimer, B. Raman Scattering from Higgs Mode Oscillations in the Two-Dimensional Antiferromagnet

- Ca₂RuO₄. *Phys. Rev. Lett.* **2017**, *119*, 067201.
- (23) Avdeev, M.; Thorogood, G. J.; Carter, M. L.; Kennedy, B. J.; Ting, J.; Singh, D. J.; Wallwork, K. S. Antiferromagnetism in a Technetium Oxide. Structure of CaTcO₃. *J. Am. Chem. Soc.* **2011**, *133*, 1654–1657.
- (24) Rodriguez, E. E.; Poineau, F.; Llobet, A.; Kennedy, B. J.; Avdeev, M.; Thorogood, G. J.; Carter, M. L.; Seshadri, R.; Singh, D. J.; Cheetham, A. K. High Temperature Magnetic Ordering in the 4d Perovskite SrTcO₃. *Phys. Rev. Lett.* **2011**, *106*, 067201.
- (25) Shi, Y. G.; Guo, Y. F.; Yu, S.; Arai, M.; Belik, A. A.; Sato, A.; Yamaura, K.; Takayama-Muromachi, E.; Tian, H. F.; Yang, H. X.; Li, J. Q.; Varga, T.; Mitchell, J. F.; Okamoto, S. Continuous metal-insulator transition of the antiferromagnetic perovskite NaOsO₃. *Phys. Rev. B* **2009**, *80*, 161104.
- (26) Calder, S.; Garlea, V. O.; McMorrow, D. F.; Lumsden, M. D.; Stone, M. B.; Lang, J. C.; Kim, J.-W.; Schlueter, J. A.; Shi, Y. G.; Yamaura, K.; Sun, Y. S.; Tsujimoto, Y.; Christianson, A. D. Magnetically Driven Metal-Insulator Transition in NaOsO₃. *Phys. Rev. Lett.* **2012**, *108*, 257209.
- (27) Wakabayashi, Y. K.; Krockenberger, Y.; Tsujimoto, N.; Boykin, T.; Tsuneyuki, S.; Taniyasu, Y.; Yamamoto, H. Ferromagnetism above 1000 K in a highly cation-ordered double-perovskite insulator Sr₃OsO₆. *Nat. Commun.* **2019**, *10*, 535.
- (28) Tian, W.; Svoboda, C.; Ochi, M.; Matsuda, M.; Cao, H. B.; Cheng, J.-G.; Sales, B. C.; Mandrus, D. G.; Arita, R.; Trivedi, N.; Yan, J.-Q. High antiferromagnetic transition temperature of the honeycomb compound SrRu₂O₆. *Phys. Rev. B* **2015**, *92*, 100404.
- (29) Hiley, C. I.; Scanlon, D. O.; Sokol, A. A.; Woodley, S. M.; Ganose, A. M.; Sangiao, S.; De Teresa, J. M.; Manuel, P.; Khalyavin, D. D.; Walker, M.; Lees, M. R.; Walton, R. I. Antiferromagnetism at $T > 500$ K in the layered hexagonal ruthenate SrRu₂O₆. *Phys. Rev. B* **2015**, *92*, 104413.
- (30) Okamoto, S.; Ochi, M.; Arita, R.; Yan, J.; Trivedi, N. Localized-itinerant dichotomy and unconventional magnetism in SrRu₂O₆. *Scientific Reports* **2017**, *7*, 11742.
- (31) Pchelkina, Z. V.; Streltsov, S. V.; Mazin, I. I. Spectroscopic signatures of molecular orbitals in transition metal oxides with a honeycomb lattice. *Phys. Rev. B* **2016**, *94*, 205148.
- (32) Ochi, M.; Arita, R.; Trivedi, N.; Okamoto, S. Strain-induced topological transition in SrRu₂O₆ and CaOs₂O₆. *Phys. Rev. B* **2016**, *93*, 195149.
- (33) Hiley, C. I.; Lees, M. R.; Fisher, J. M.; Thompsett, D.; Agrestini, S.; Smith, R. I.; Walton, R. I. Ruthenium(V) Oxides from Low-Temperature Hydrothermal Synthesis. *Angew. Chem. Int. Ed.* **2014**, *53*, 4423.
- (34) Kane, C. L.; Mele, E. J. Z₂ Topological Order and the Quantum Spin Hall Effect. *Phys. Rev. Lett.* **2005**, *95*, 146802.
- (35) Haldane, F. D. M. Model for a Quantum Hall Effect without Landau Levels: Condensed-Matter Realization of the "Parity Anomaly". *Phys. Rev. Lett.* **1988**, *61*, 2015–2018.
- (36) Zhang, Y.; Tan, Y.-W.; Stormer, H. L.; Kim, P. Experimental observation of the quantum Hall effect and Berry's phase in graphene. *Nature* **2005**, *438*, 201–204.
- (37) Banerjee, A. et al. Proximate Kitaev quantum spin liquid behaviour in a honeycomb magnet. *Nature Materials* **2016**, *15*, 733 EP –, Article.

- (38) Sears, J. A.; Songvilay, M.; Plumb, K. W.; Clancy, J. P.; Qiu, Y.; Zhao, Y.; Parrishall, D.; Kim, Y.-J. Magnetic order in $\alpha - \text{RuCl}_3$: A honeycomb-lattice quantum magnet with strong spin-orbit coupling. *Phys. Rev. B* **2015**, *91*, 144420.
- (39) Choi, S. K.; Coldea, R.; Kolmogorov, A. N.; Lancaster, T.; Mazin, I. I.; Blundell, S. J.; Radaelli, P. G.; Singh, Y.; Gegenwart, P.; Choi, K. R.; Cheong, S.-W.; Baker, P. J.; Stock, C.; Taylor, J. Spin Waves and Revised Crystal Structure of Honeycomb Iridate Na_2IrO_3 . *Phys. Rev. Lett.* **2012**, *108*, 127204.
- (40) Jackeli, G.; Khaliullin, G. Mott Insulators in the Strong Spin-Orbit Coupling Limit: From Heisenberg to a Quantum Compass and Kitaev Models. *Phys. Rev. Lett.* **2009**, *102*, 017205.
- (41) Singh, Y.; Gegenwart, P. Antiferromagnetic Mott insulating state in single crystals of the honeycomb lattice material Na_2IrO_3 . *Phys. Rev. B* **2010**, *82*, 064412.
- (42) Gupta, S. N.; Sriluckshmy, P. V.; Mehlawat, K.; Balodhi, A.; Mishra, D. K.; Hassan, S. R.; Ramakrishnan, T. V.; Muthu, D. V. S.; Singh, Y.; Sood, A. K. Raman signatures of strong Kitaev exchange correlations in $(\text{Na}_{1-x}\text{Li}_x)_2\text{IrO}_3$: Experiments and theory. *EPL (Europhysics Letters)* **2016**, *114*, 47004.
- (43) Knolle, J.; Chern, G.-W.; Kovrizhin, D. L.; Moessner, R.; Perkins, N. B. Raman Scattering Signatures of Kitaev Spin Liquids in $A_2\text{IrO}_3$ Iridates with $A = \text{Na}$ or Li . *Phys. Rev. Lett.* **2014**, *113*, 187201.
- (44) Streltsov, S.; Mazin, I. I.; Foyevtsova, K. Localized itinerant electrons and unique magnetic properties of SrRu_2O_6 . *Phys. Rev. B* **2015**, *92*, 134408.
- (45) J., T.; Gemming T, e. b. M. J. e. a. *Proceedings of the EMC2008: 14th European Microscopy Congress*; ISBN 978-3-540-85301-5, 2008.
- (46) Nicolosi, V.; Chhowalla, M.; Kanatzidis, M. G.; Strano, M. S.; Coleman, J. N. Liquid Exfoliation of Layered Materials. *Science* **2013**, *340*.
- (47) Griffin, A.; Harvey, A.; Cunningham, B.; Scullion, D.; Tian, T.; Shih, C.-J.; Gruening, M.; Donegan, J. F.; Santos, E. J. G.; Backes, C.; Coleman, J. N. Spectroscopic Size and Thickness Metrics for Liquid-Exfoliated h-BN. *Chemistry of Materials* **2018**, *30*, 1998–2005.
- (48) Ogilvie, S. P.; Large, M. J.; Fratta, G.; Meloni, M.; Canton-Vitoria, R.; Tagmatarchis, N.; Massuyeau, F.; Ewels, C. P.; King, A. A. K.; Dalton, A. B. Considerations for spectroscopy of liquid-exfoliated 2D materials: emerging photoluminescence of N-methyl-2-pyrrolidone. *Scientific Reports* **2017**, *7*, 16706.
- (49) Backes, C. et al. Edge and confinement effects allow in situ measurement of size and thickness of liquid-exfoliated nanosheets. *Nature Communications* **2014**, *5*, 4576 EP –, Article.
- (50) Puthirath Balan, A. et al. Exfoliation of a non-van der Waals material from iron ore hematite. *Nature Nanotechnology* **2018**, *13*, 602–609.
- (51) Osada, M.; Sasaki, T. Two-Dimensional Dielectric Nanosheets: Novel Nanoelectronics From Nanocrystal Building Blocks. *Advanced Materials* **2012**, *24*, 210–228.
- (52) Sun, Z.; Liao, T.; Dou, Y.; Hwang, S. M.; Park, M.-S.; Jiang, L.; Kim, J. H.; Dou, S. X. Generalized self-assembly of scalable two-dimensional transition metal oxide nanosheets. *Nature Communications* **2014**, *5*, 3813 EP –, Article.

- (53) Aksit, M.; Toledo, D. P.; Robinson, R. D. Scalable nanomanufacturing of millimetre-length 2D Na_xCoO_2 nanosheets. *J. Mater. Chem.* **2012**, *22*, 5936–5944.
- (54) Ponosov, Y. S.; Komleva, E. V.; Zamyatin, D. A.; Walton, R. I.; Streltsov, S. V. Raman spectroscopy of the low-dimensional antiferromagnet SrRu_2O_6 with large Néel temperature. *Phys. Rev. B* **2019**, *99*, 085103.
- (55) Pulickel Ajayan, P. K.; Banerjee, K. Two-dimensional van der Waals materials. *Physics Today* **2016**, *69*, 38.
- (56) Kim, K.; DaSilva, A.; Huang, S.; Fallahzad, B.; Larentis, S.; Taniguchi, T.; Watanabe, K.; LeRoy, B. J.; MacDonald, A. H.; Tutuc, E. Tunable moiré bands and strong correlations in small-twist-angle bilayer graphene. *Proceedings of the National Academy of Sciences* **2017**, *114*, 3364–3369.
- (57) Yoo, H. et al. Atomic and electronic reconstruction at the van der Waals interface in twisted bilayer graphene. *Nature Materials* **2019**, *18*, 448–453.
- (58) Warner, J. H.; Rümmeli, M. H.; Gemming, T.; Büchner, B.; Briggs, G. A. D. Direct Imaging of Rotational Stacking Faults in Few Layer Graphene. *Nano Lett.* **2009**, *9*, 102–106.
- (59) Kresse, G.; Hafner, J. Ab initio molecular dynamics for liquid metals. *Phys. Rev. B* **1993**, *47*, 558–561.
- (60) Kresse, G.; Furthmüller, J. Efficient iterative schemes for ab initio total-energy calculations using a plane-wave basis set. *Phys. Rev. B* **1996**, *54*, 11169–11186.
- (61) Blöchl, P. E. Projector augmented-wave method. *Phys. Rev. B* **1994**, *50*, 17953–17979.
- (62) Perdew, J. P.; Burke, K.; Ernzerhof, M. Generalized Gradient Approximation Made Simple. *Phys. Rev. Lett.* **1996**, *77*, 3865–3868.
- (63) Tian, W.; Svoboda, C.; Ochi, M.; Matsuda, M.; Cao, H. B.; Cheng, J.-G.; Sales, B. C.; Mandrus, D. G.; Arita, R.; Trivedi, N.; Yan, J.-Q. High antiferromagnetic transition temperature of the honeycomb compound SrRu_2O_6 . *Phys. Rev. B* **2015**, *92*, 100404.
- (64) Suzuki, H. et al. Spin waves and spin-state transitions in a ruthenate high-temperature antiferromagnet. *Nature Materials* **2019**,
- (65) Singh, D. J. Electronic structure and the origin of the high ordering temperature in SrRu_2O_6 . *Phys. Rev. B* **2015**, *91*, 214420.
- (66) Hariki, A.; Hausoel, A.; Sangiovanni, G.; Kuneš, J. DFT+DMFT study on soft moment magnetism and covalent bonding in SrRu_2O_6 . *Phys. Rev. B* **2017**, *96*, 155135.